3D Visualisation of trans-syncytial nanopores provides a pathway for paracellular diffusion across the human placental syncytiotrophoblast

Short title: Trans-syncytial nanopores

Rohan M Lewis*[1,3], Harikesan Baskaran[4], Jools Green[1], Stanimir Tashev[2], Eleni Paleologou[1], Emma M Lofthouse[1], Jane K Cleal[1,3], Anton Page[2], David S Chatelet[2], Patricia Goggin[2], Bram G Sengers[3,4]

[1] University of Southampton, Faculty of Medicine

[2] University of Southampton, Faculty of Medicine, Biomedical Imaging Unit

[3] University of Southampton, Institute for Life Sciences

[4] University of Southampton, Faculty of Engineering and Physical Sciences

***Corresponding Author**: Rohan M Lewis, MP 887, IDS Building University of Southampton, Faculty of Medicine, Southampton General Hospital, rohan.lewis@soton.ac.uk

Abstract

The placental syncytiotrophoblast, a syncytium without cell-cell junctions, is the primary barrier between the mother and the fetus. Despite no apparent anatomical pathway for paracellular diffusion of solutes across the syncytiotrophoblast size-dependent paracellular diffusion is observed. Here we report data demonstrating that the syncytiotrophoblast is punctuated by trans-syncytial nanopores (TSNs). These membrane-bound TSNs directly connect the maternal and fetal facing sides of the syncytiotrophoblast, providing a pathway for paracellular diffusion between the mother and fetus. Mathematical modelling of TSN permeability based on their 3D geometry suggests that 10-60 million TSNs per cm^3 of placental tissue could explain experimentally observed placental paracellular diffusion. TSNs may mediate physiological hydrostatic and osmotic pressure homeostasis between the maternal and fetal circulations but also expose the fetus to pharmaceuticals, environmental pollutants and nanoparticles.

Introduction

The placenta was once viewed as a perfect barrier, but as the thalidomide tragedy demonstrated, this is not the case [1]. It is now clear that potentially harmful molecules and particulates can cross the placenta and adversely affect fetal development. However, the mechanism by which these molecules and particulates cross the placenta is not always clear [2, 3]. Understanding how these substances cross the placenta is necessary to identify the risks and prevent long-term consequences of these exposures, which may adversely affect fetal and postnatal health [4].

The primary placental barrier is the syncytiotrophoblast, a continuous syncytial monolayer covering the villi at the maternal-fetal interface. As there are no cell-cell junctions in a syncytium, there is no obvious pathway by which paracellular diffusion can occur. Despite the absence of an anatomical pathway for diffusion, there is physiological evidence for size-dependent paracellular diffusion of solutes [5, 6]. Trans-syncytial channels, or nanopores, have been proposed as mediators of trans-syncytial diffusion, however continuous full-width nanopores have not been previously demonstrated in the human placenta [7]. An alternative hypothesis to explain paracellular diffusion is that it occurs through regions of syncytial damage [8]. These hypotheses are not mutually exclusive but establishing mechanisms of fetal exposure is necessary to understand the likely risks of different compounds and develop strategies to mitigate this.

Selective placental transfer of nutrients, IgG, wastes and exogenous toxins is facilitated by membrane transporters and endocytosis [9-11]. However it is not clear how exogenous drugs and toxins reach the fetus as, with a few exceptions such as the apically located exchanger OATP4A1 [10], drug transporters in the placenta mediate efflux from the fetus to the mother [12]. Nanoparticle transfer across the placenta has been observed, but the mechanism is unclear [13]. A more extensive understanding of how metabolites, pharmaceuticals and toxins reach the fetal circulation is necessary to protect fetal health.

Estimates of placental permeability surface area products for hydrophilic solutes have been determined *in vivo* and show size-dependent permeability of solutes, which decreases with increasing molecular radius [5, 6]. In other species with haemochorial placentas, permeability has also been shown to be size-selective with some species having higher or lower overall permeability compared to humans [3, 14]. This data suggests a size-selective permeability of the placenta through low diameter channels [15].

Using serial block-face scanning electron microscopy (SBF SEM) to reconstruct placental ultrastructure in three dimensions, this study demonstrates the presence of full-width trans-syncytial nanopores (TSNs) in the human placenta.

Methods

Term placental tissue was collected after delivery from uncomplicated pregnancies with written informed consent and ethical approval from the Southampton and Southwest Hampshire Local Ethics Committee (11/SC/0529).

Tissue collection and fixation for electron microscopy

Villous samples from 8 placentas were collected as soon as possible after delivery and small pieces (≈ 2 mm^3) fixed in 3% glutaraldehyde in 0.1 M cacodylate buffer at pH 7.4 at RT and then stored at 4°C for > 24 hours before processing for either SBF SEM or transmission electron microscopy (TEM).

TEM processing and imaging

Fixed placental fragments were washed twice for 10 min in 0.1 M sodium cacodylate buffer (Agar Scientific, UK) at pH 7.4 containing 0.23 M sucrose (BDH, UK) and 2 mM $CaCl_2$ (BDH, UK). The specimens were incubated for 60 min in 2% osmium tetroxide (BDH, UK), in 0.1 M sodium cacodylate (Agar Scientific, UK) at pH 7.4, then washed three times for 10 min with distilled water. Samples were then treated with 2% aqueous uranyl acetate (Agar Scientific, UK) for 20 min. Samples were dehydrated using a graded ethanol series. Specimens were then treated with 50:50 Spurr resin:acetonitrile (Fisher, UK) overnight and then infiltrated with fresh Spurr resin for 6 h. Finally, specimens were embedded in Spurr resin for 16 h at 60°C. Gold/ silver ultrathin sections were cut using a Reichert Ultracut E ultramicrotome, stained with Reynolds lead citrate and viewed by TEM (Tecnai 12, ThermoFisher, Eindhoven).

SBF SEM processing and imaging

SBF SEM is a high-resolution technique where serial images are generated from a resin block which is sliced sequentially by an automated ultramicrotome in the chamber of a scanning electron microscope. Fixed samples for SBF SEM were processed based on Deerinck et al. [16] as adapted in our laboratory [17]. Blocks were imaged using a Gatan 3View (Gatan, Abingdon, UK) inside a FEI Quanta 250 FEGSEM (ThermoFisher, Eindhoven, Netherlands) at 3.0 kV accelerating voltage, spot size 3 and with a vacuum level of 40 Pa. Stacks of images were collected at pixel size from 4-7 nm with slice thickness ranging 25-50 nm.

Identification and segmentation trans-syncytial nanopores

SBF SEM image stacks of terminal or intermediate villi were processed in Fiji (version 2.0.0-rc-43) using a Gaussian blur filter (sigma radius 2) and enhance contrast function (0.4% saturated pixels) [18]. Continuous TSNs were identified where there was a clear connection between the apical and basal membrane. Near-continuous TSNs were also identified which had connections to both the apical microvillous and basal plasma membranes but along the length of the nanopore contained discontinuities, where the ends of the discontinuous sections were adjacent (Figure 1). In addition, unilateral nanopores were identified which were ultrastructurally similar to TSNs opened from either the apical or basal plasma

membrane but did not appear to connect to the opposite membrane, ending within the cytoplasm. Selected regions containing TSNs were manually segmented in Avizo v2019.4 (ThermoFisher, Eindhoven).

Modelling of nanopore diffusive transfer capacity

According to Fick's first law, the magnitude of the diffusive flux J_{pore} [mol/s] through a pore of uniform cross section is given by:

$$J_{pore} = DA_{pore}\frac{|\Delta C|}{L_{pore}} \qquad \text{Eq. 1}$$

where D [m^2/s] is the diffusion coefficient, A_{pore} [m^2] the pore cross sectional area, ΔC [mol/m^3] the concentration difference over the pore and L_{pore} [m] the pore length. This can also be expressed in terms of permeability surface area product PS_{pore} [m^3/s] of the pore:

$$J_{pore} = PS_{pore}\Delta C \quad \text{, where } PS_{pore} = \frac{DA_{pore}}{L_{pore}} \qquad \text{Eq. 2}$$

Since in reality the pore cross sectional area varies, 3D image-based simulations were used to calculate the effective area over length ratio A_{pore}/L_{pore} [m] as a measure for the effect of pore geometry on diffusive transfer, independent of the solute studied.

For each pore, previously segmented image stacks were imported in Simpleware ScanIP (P-2019.09; Synopsys, Inc., Mountain View, USA) to reconstruct the 3D pore geometry. Because of the non-isotropic voxels, voxels were resampled isotropically so that the x and y pixel size matched the z axis spacing. Pore inlet and outlet surfaces were defined, after which the pore was meshed using linear tetrahedral elements to enable subsequent simulations of diffusive transfer using the Finite Element method. Different coarseness settings were evaluated, with the final number of elements used for the different pores ranging from 1.4–38×10^5.

Steady state diffusion simulations were performed in COMSOL Multiphysics (v5.5; COMSOL AB, Stockholm, Sweden) using the pore mesh exported from Simpleware. Since the choice of parameters does not affect the final result for A_{pore}/L_{pore}, a diffusion coefficient of 1 m^2/s was used and a fixed concentration gradient was imposed by prescribing constant concentration boundary conditions of 1 and 0 [mol/m^3] on the inlet and outlet surface of the pore, respectively. The remaining external surface of the pore was subject to no-flux boundary conditions.

After simulations were completed, the magnitude of the diffusive flux J_{pore} was calculated using the integral of the normal solute flux over the pore inlet or outlet cross sectional area. In combination with the imposed concentration difference ΔC and diffusion coefficient D used in the simulation, the value for J_{pore} was then used to calculate the effective pore area over length ratio A_{pore}/L_{pore} based on Eq. 1.

Results

Trans-syncytial nanopores

This study manually inspected 14 SBF SEM image stacks from five different placentas to identify trans-syncytial nanopores (TSNs) defined as membrane lined pores connecting the apical and basal plasma membranes of the syncytiotrophoblast. These stacks consisted of 7487 SBF SEM images, representing a total imaged volume of 0.000002 cm^3.

Inspection of serial sections allowed identification of TSNs crossing the syncytiotrophoblast (figure 2). Ten continuous TSNs were identified from three different placentas. In addition, 20 near-continuous TSNs were identified, with examples in all five placentas studied. In two cases, these near-continuous TSNs were highly complicated with branches, multiple dilations, and blind ends (figure 3b). Finally, 25 unilateral nanopores were identified arising from either the apical (n = 17) or basal (n = 8) plasma membrane of the syncytiotrophoblast but not connecting to the opposing plasma membrane.

The TSNs were structurally heterogeneous, ranging from simple thin tubes connecting the apical and basal syncytiotrophoblast plasma membranes to complex branching structures with multiple dilated regions and blind ends (figures 3b, 3e and 4). The more complex TSNs will have lower permeability raising the question as to whether they have roles in addition to mediating diffusion.

The lumens of TSNs typically had a low electron density, consistent with a primarily fluid filled pore (figure 2). However, some TSNs and regions of TSNs were observed with higher electron density indicating diffuse contents (figure 2e). The electron density of TSN lumens was typically lower than of endocytic vesicles (figure 5).

The TSN openings did not appear to have structures reminiscent of dynamin spirals or clathrin-coated vesicles although these structures may not be apparent on SBF SEM images (figure 5k). The electron densities within the void space of TSN openings were typically lower than in syncytiotrophoblast endocytic vesicles.

On the basal membrane, continuous and near-continuous TSN were observed opening adjacent to basal lamina in 16 cases and regions adjacent to cytotrophoblast in 14 cases.

Of the ten continuous TSNs, eight contained membrane-bound inclusions which, surrounded by pore membrane, formed double-membrane structures (figure 3). Inclusions were also observed in the majority of near-continuous and unilateral nanopores. In three cases, the inclusions appeared to be trophoblastic in origin. In the first case, the inclusion on the apical side appeared to be connected to the syncytiotrophoblast by at least one thin stalk of cytoplasmic material (figure 3a). At the available resolution, it was not clear whether other inclusions were also engulfed syncytiotrophoblast. In two cases, an inclusion on the basal side of the placenta was a clear-cut protrusion from an underlying cytotrophoblast cell (figure 3d).

Thin desmosome containing nanopores

Another less commonly observed feature associated with TSNs were thin nanopores within the syncytiotrophoblast, where two closely adjacent membranes were joined by desmosome like adhesions (figure 6). These were observed in two TEM images and one SBFSEM image stack. In one case a desmosome associated nanopore was seen almost crossing the placenta from the basal membrane to near the microvillous membrane (figure 6a). Desmosome associated nanopores were observed in one SBF SEM image stack where they were found to be ribbon or sheet-like structures 5-16 nm wide and estimated at 200-800 nm deep (figure 6b). Desmosome containing nanopores could be seen appearing and disappearing within the same 2D section, which is consistent with a pore rather than a cell-cell junction. Topologically a cell-cell junction would need to either interact with two cell or image boundaries or form a circular feature (figure 6c).

Modelling diffusion through TSNs

Depending on their geometry, individual nanopores display a large variation in estimated effective A_{pore}/L_{pore} from 0.14 x 10^{-8} m to 2.08 x 10^{-8} m (figure 4j). The effective A_{pore}/L_{pore} ratio based on the results of the computational simulations of the ten pores, as depicted in Figure 3, was in the order of 10 nm (8.5 ± 7.2 × 10^{-9} m, mean ± SD). By multiplying the mean effective A_{pore}/L_{pore} ratio with the diffusion coefficient for particular solutes using Eq. 2, the average permeability surface area products for a single pore could then be calculated (Table 1). Dividing the corresponding experimentally observed placental permeability surface area products by the value for a single pore, resulted in placental pore number estimates between 13 and 59 million pores per gram.

Discussion

The demonstration of nanoscale pores punctuating the syncytiotrophoblast challenges our understanding of the placenta as a barrier. It suggests that rather than being a continuous physical barrier between mother and fetus, the syncytiotrophoblast is a molecular sieve facilitating the diffusion of small solutes via the active maintenance of TSNs. Small solutes that may diffuse via TSNs include nutrients, metabolites and toxins, so transfer via this route may have profound implications for the fetus. While this study demonstrates the existence of TSNs and modelling suggests that they are likely to have the capacity to mediate physiologically significant transfer, further work is needed to establish their numbers, distribution and whether these change in disease states.

In 2D images the TSNs typically had a small profile, making it difficult to visualize their relation to other structures and therefore making it difficult to identify them as TSNs. When reconstructed in 3D, the TSNs were structurally heterogeneous, including simple tubes, tubes with apparently empty dilated regions and branched structures with blind ends. Many TSNs also contained inclusions of membrane-bound material. Some TSNs had multiple openings to the syncytiotrophoblast apical microvillous or basal membranes. In addition to continuous TSNs, near-continuous TSNs and unilateral nanopores were observed, which based on ultrastructural similarities we believe to be related. In addition, the presence of inclusions supports our contention that continuous TSNs, near-continuous TSNs and unilateral nanopores, are related structures. These near-continuous and unilateral nanopores are likely to be in the process of formation, degradation or remodelling. For near-continuous TSNs, it is also possible that these are continuous but that the connections were too thin to observe. The relatively large number of near-continuous and unilateral nanopores is consistent with TSNs being dynamically remodelled, and studies in live cells are required to study TSN formation, turnover and regulation.

On the basal membrane, around half of TSN opened adjacent to the basal lamina and half adjacent to cytotrophoblast cells. However, as cytotrophoblast occupy only 30% of the basal lamina, there may be a preference for TSNs opening adjacent to cytotrophoblast cells [19]. TSNs opening to the basal lamina would release solutes directly into the villous stroma providing the most direct pathway to the fetal circulation. Solutes diffusing through TSN openings above cytotrophoblast cells could diffuse between these cells to the fetus or be taken up by the cytotrophoblast cells. While this remains speculation, TSNs opening adjacent to cytotrophoblast may also provide a direct route by which cytotrophoblast could either sense maternal environment or signal to it.

There was a wide range in calculated permeability parameters for the modelled TSNs, with diffusion through the most permeable being 10 x greater than the least permeable. As might be expected, shorter, wider TSNs had the greatest permeability while the longer TSNs had the lowest permeability (excluding the TSN with multiple apical and basal openings).

Paracellular diffusion across the placenta is size-selective, but the TSNs are likely to be too wide to impose this size selectivity on smaller molecules. Physiological estimates of

placental pore sizes in rodents are in the order of 17 nm, which is consistent with the thinnest regions of the nanopores described here and with the desmosome associated channels we observed [15]. For comparison glucose is 1.5 nm long so should diffuse freely though pores of this size. If the TSNs do not impose size selectivity, other structures such as the trophoblast basal lamina or the fetal capillary might [20]. If these structures and not the syncytiotrophoblast impose size selectivity, this again represents a significant shift in our understanding of the placental barrier, and the permeability of these other structures require further investigation. Our permeability estimate was based on nanopores through the syncytiotrophoblast alone, while the different layers may impose additional restrictions and reduce permeability, thereby increasing the number of pores required.

Larger molecules such as IgG or nanoparticles such as ultrafine diesel exhaust could fit through most regions of the TSNs, but the diameter would provide steric hindrance to their transfer. TSN diameter might be a significant barrier to the transfer of large molecules unless an additional biological mechanism facilitates this transfer.

Further research is required to determine TSN densities in placental tissue accurately. An initial approximation for the TSN density was obtained by dividing the number of observed TSNs (10 continuous or 30 including continuous and near-continuous TSNs) by the imaged volume of 0.000002 cm^3. Therefore, this initial approximation for TSN density is 51 million TSNs per cm^3 of placental tissue, and including near-continuous TSNs is 143 million/cm^3. How accurate this estimate is will depend on how many TSNs were present but missed by the investigators and how representative the tissue in the electron microscopy blocks is of the placenta as a whole. However, this estimate is in line with the number of TSNs required to mediate the transfer of known paracellular markers such as inulin and creatinine.

The presence of membrane-bound inclusions within the TSNs suggests their role could be more complex than simply being pores for diffusion. The nanopore inclusions and surrounding TSN membrane create a double membrane structure which shows some ultrastructural similarities to 2D images of autophagosomes [21]. Nanopore inclusions can be observed in a previous study that sought to identify TSNs using lanthanum perfusion [7]. In that study, adjacent, nanopore inclusions can be seen where one inclusion is stained with lanthanum and the other is not, consistent with our suggestion that nanopores are dynamic structures.

In some cases, the inclusions appeared trophoblastic in origin. In the first case, the inclusion on the apical side appeared to be connected to the syncytiotrophoblast by at least one thin stalk of cytoplasmic material. This is consistent with syncytiotrophoblast having been pinched off into a nanopore inclusion and could potentially represent the initiation of autophagy or material that will be shed from the placenta. In other cases, inclusions on the basal side of the placenta were observed to be protrusions from underlying cytotrophoblast cells. The role of these cytotrophoblast inclusions is unclear, but it could potentially allow direct sensing of the maternal environment. It is possible that the remaining inclusions are

also of trophoblastic origin but that the images we have were not clear enough to demonstrate this.

Whether there is any relationship between TSNs and the endocytic process in terms of mechanisms or function is unclear. The TSNs did not appear to have structures reminiscent of dynamin spirals or clathrin-coated vesicles. However, higher-resolution 3D imaging is necessary to address this question. TSNs may be related to structures produced by clathrin-independent carriers (CLIC) and GPI-anchored protein-enriched early endosomal compartment (GEEC) pathways [22]. The CLIC/GEEC pathways form uncoated tubulovesicular membrane structures and identifying whether these or other molecular mechanisms underly TSN formation will be necessary for determining regulation and function [23]. It should be noted that in a 2D z slice, the TSNs can look like cytoplasmic endocytic vesicles.

A rare feature associated with TSNs was desmosome associated nanopores which were most commonly observed arising from basal membrane folds [19], but were also observed within the cytoplasm. While no desmosome associated nanopores were observed connecting to the microvillous membrane, they did connect to TSN like structures, and it is possible that these represent a stage in TSN creation or removal. These desmosome associated nanopores have been observed previously and it has been suggested that they are remnants of cytotrophoblast-syncytiotrophoblast fusion which is another possibility [24]. Whatever their origin, the desmosome containing nanopores could be acting as conduits for paracellular diffusion in conjunction with or alongside TSNs. As the desmosome associated nanopores are so thin, they may only be clearly visualised when the block is in specific orientations, and so they may be more common than it appears. Cells that cross or penetrate epithelial barriers have been observed to express tight junction proteins to facilitate movement through cell-cell junctions, and the desmosome containing nanopores in the syncytiotrophoblast could provide a route and a mechanism by which maternal or fetal cells could cross the syncytiotrophoblast [25, 26]. Images of erythrocytes protruding through the syncytiotrophoblast suggest that distensible channels that could allow cell passage exist [27].

The physiological role of TSNs is likely to include the maintenance of ionic and osmotic homeostasis between the mother and fetus. Diffusion of ions and bulk flow of fluid would balance any osmotic and pressure gradients that could otherwise build up across the placenta if the syncytiotrophoblast did not allow paracellular diffusion. TSNs may also facilitate the placental transfer of nutrients, such as glucose, with maternal to fetal gradients to the fetus. Diffusion of glucose via TSNs may explain why attempts to inhibit placental glucose transfer competitively have been unsuccessful [28]. However, the physiological roles of TSNs may come at the cost of allowing non-selective placenta transfer of potentially harmful substances and reducing the efficiency of active nutrient transport. For nutrients whose concentration is higher in fetal than maternal plasma, such as amino acids, TSNs may mediate leak back to the mother, reducing the efficiency of active transfer. Nutrients bound to binding proteins, e.g. calcium and vitamin D will be less susceptible to

back flux via the TSNs. The TSNs also provide a pathway for potentially harmful molecules to cross the placenta, including pharmacological drugs, environmental toxins, nanoparticles and maternal wastes. Efflux transporters and organic cation and anion transporters act together to pump toxins in the fetal to maternal direction. However, it is less clear how the fetus is exposed to exogenous toxins in the first place, and the identification of TSNs suggests that water-soluble toxins could diffuse across the placental barrier.

Structures similar to the TSNs could play essential roles in other tissues, particularly epithelial or endothelial barriers. Trans-endothelial pores have been reported in mouse endothelial cells where they may play a role in capillary permeability [29]. We have also reported an example of a large pore in human placental endothelium [30].

There is considerable diversity in placental structures across species and given the possibility that the syncytiotrophoblast has evolved independently in different branches of the evolutionary tree, the diversity of TSNs (or similar structures) is of interest. To date, full width trans-syncytial channels have only been described in the degu which has both short direct channels in thin regions of syncytiotrophoblast and more complex channels connecting infoldings of basal and apical surfaces [31]. The human TSNs had a distinct appearance but were most similar to the more complex Degu channels, although longer and thinner. The distribution of TSNs across species may inform their biological role and origins.

Identifying the molecular processes underlying TSN formation will be key to understanding these structures. While TSNs may form by a unique mechanism, they are more likely to co-opt at least some of the known molecular mechanisms that mediate endocytosis. There are multiple endocytic processes, including clathrin and caveolin, micropinosomes or CLIC/GEEC, which form tubular structures [23]. The CLIC/GEEC may be of particular interest as these form tube-like structures [32].

In conclusion use of three-dimensional imaging approaches has demonstrated the existence of TSNs. These TSNs will mediate non-selective diffusion across the placenta and may be the pathway by which pharmacological drugs, environmental toxins and even particulate pollutants cross the syncytiotrophoblast. In the future, accurately determining the density of TSNs in healthy pregnancy is necessary to confirm the capacity of TSNs to mediate transfer. Furthermore, establishing the density of TSNs in disease states may provide novel insights into disease processes.

Acknowledgements: This work was supported by BBSRC project grant BB/R002762/1. Equipment in the Biomedical Imaging Unit was supported by MR/L012626/1 Southampton Imaging under MRC UKRMP Funding.

Competing interests: None

Author contributions CREDIT statement

Rohan M Lewis: Conceptualization, Funding Acquisition, Investigation, Supervision, Writing – Original Draft Preparation, Writing – Review & Editing.

364 Harikesan Baskaran: Investigation, Formal Analysis, Writing – Review & Editing.
365 Jools Green: Investigation, Writing – Review & Editing.
366 Stanimere Tashev: Investigation, Writing – Review & Editing.
367 Eleni Paleologou: Investigation, Writing – Review & Editing.
368 Emma M Lofthouse: Resources, Writing – Review & Editing.
369 Jane K Cleal: Funding Acquisition, Supervision, Writing – Review & Editing.
370 Anton Page: Funding Acquisition, Methodology, Supervision, Writing – Review & Editing.
371 David S Chatelet: Formal Analysis, Supervision, Writing – Review & Editing.
372 Patricia Goggin: Methodology, Supervision, Writing – Review & Editing.
373 Bram G Sengers: Funding Acquisition, Formal Analysis, Supervision, Writing – Original Draft
374 Preparation, Writing – Review & Editing.

References

1. Dally A. Thalidomide: was the tragedy preventable? Lancet. 1998;351(9110):1197-9. Epub 1998/06/27. doi: 10.1016/S0140-6736(97)09038-7. PubMed PMID: 9643709.

2. Lofthouse EM, Torrens C, Manousopoulou A, Nahar M, Cleal JK, O'Kelly IM, et al. Ursodeoxycholic acid inhibits uptake and vasoconstrictor effects of taurocholate in human placenta. FASEB journal : official publication of the Federation of American Societies for Experimental Biology. 2019;33(7):8211-20. Epub 2019/03/30. doi: 10.1096/fj.201900015RR. PubMed PMID: 30922127; PubMed Central PMCID: PMCPMC6593889.

3. Bove H, Bongaerts E, Slenders E, Bijnens EM, Saenen ND, Gyselaers W, et al. Ambient black carbon particles reach the fetal side of human placenta. Nat Commun. 2019;10(1):3866. Epub 2019/09/19. doi: 10.1038/s41467-019-11654-3. PubMed PMID: 31530803; PubMed Central PMCID: PMCPMC6748955.

4. Lewis RM, Demmelmair H, Gaillard R, Godfrey KM, Hauguel-de Mouzon S, Huppertz B, et al. The Placental Exposome: Placental Determinants of Fetal Adiposity and Postnatal Body Composition. Annals of Nutrition and Metabolism. 2013;63(3):208-15. doi: 10.1159/000355222. PubMed PMID: WOS:000329057400005.

5. Thornburg KL, Burry KJ, Adams AK, Kirk EP, Faber JJ. Permeability of placenta to inulin. American journal of obstetrics and gynecology. 1988;158(5):1165-9. Epub 1988/05/01. doi: 10.1016/0002-9378(88)90246-3. PubMed PMID: 3369499.

6. Bain MD, Copas DK, Taylor A, Landon MJ, Stacey TE. Permeability of the human placenta in vivo to four non-metabolized hydrophilic molecules. The Journal of physiology. 1990;431:505-13. PubMed PMID: 2129229; PubMed Central PMCID: PMCPMC1181787.

7. Kertschanska S, Kosanke G, Kaufmann P. Pressure dependence of so-called transtrophoblastic channels during fetal perfusion of human placental villi. Microscopy research and technique. 1997;38(1-2):52-62. doi: 10.1002/(SICI)1097-0029(19970701/15)38:1/2<52::AID-JEMT7>3.0.CO;2-W. PubMed PMID: 9260837.

8. Brownbill P, Mahendran D, Owen D, Swanson P, Thornburg KL, Nelson DM, et al. Denudations as paracellular routes for alphafetoprotein and creatinine across the human syncytiotrophoblast. American journal of physiology Regulatory, integrative and comparative physiology. 2000;278(3):R677-83. PubMed PMID: 10712288.

9. Cleal JK, Glazier JD, Ntani G, Crozier SR, Day PE, Harvey NC, et al. Facilitated transporters mediate net efflux of amino acids to the fetus across the basal membrane of the placental syncytiotrophoblast. The Journal of physiology. 2011;589(4):987-97. doi: 10.1113/jphysiol.2010.198549. PubMed PMID: WOS:000287743400026.

10. Lofthouse EM, Cleal JK, O'Kelly IM, Sengers BG, Lewis RM. Estrone sulphate uptake by the microvillous membrane of placental syncytiotrophoblast is coupled to glutamate efflux. Biochem Biophys Res Commun. 2018;506(1):237-42. Epub 2018/10/23. doi: 10.1016/j.bbrc.2018.10.074. PubMed PMID: 30343886.

11. Firan M, Bawdon R, Radu C, Ober RJ, Eaken D, Antohe F, et al. The MHC class I-related receptor, FcRn, plays an essential role in the maternofetal transfer of gamma-globulin in humans. Int Immunol. 2001;13(8):993-1002. Epub 2001/07/27. doi: 10.1093/intimm/13.8.993. PubMed PMID: 11470769.

12. Iqbal M, Audette MC, Petropoulos S, Gibb W, Matthews SG. Placental drug transporters and their role in fetal protection. Placenta. 2012;33(3):137-42. Epub 2012/01/24. doi: 10.1016/j.placenta.2012.01.008. PubMed PMID: 22265855.

13. Gruber MM, Hirschmugl B, Berger N, Holter M, Radulovic S, Leitinger G, et al. Plasma proteins facilitates placental transfer of polystyrene particles. J Nanobiotechnology.

2020;18(1):128. Epub 2020/09/11. doi: 10.1186/s12951-020-00676-5. PubMed PMID: 32907583; PubMed Central PMCID: PMCPMC7487953.

14. Sibley CP. Understanding placental nutrient transfer--why bother? New biomarkers of fetal growth. The Journal of physiology. 2009;587(Pt 14):3431-40. doi: 10.1113/jphysiol.2009.172403. PubMed PMID: 19417095; PubMed Central PMCID: PMC2742272.

15. Stulc J. Extracellular transport pathways in the haemochorial placenta. Placenta. 1989;10(1):113-9. Epub 1989/01/01. PubMed PMID: 2654915.

16. Deerinck TJ, Bushong EA, Lev-Ram V, Shu X, Tsien RY, Ellisman MH. Enhancing serial block-face scanning electron microscopy to enable highresolution 3-D nanohistology of cellsandtissues. Microsc Microanal. 2010; 16:1138–9.

17. Palaiologou E, Etter O, Goggin P, Chatelet DS, Johnston DA, Lofthouse EM, et al. Human placental villi contain stromal macrovesicles associated with networks of stellate cells. Journal of anatomy. 2020;236(1):132-41. Epub 2019/09/13. doi: 10.1111/joa.13082. PubMed PMID: 31512233.

18. Schindelin J, Arganda-Carreras I, Frise E, Kaynig V, Longair M, Pietzsch T, et al. Fiji: an open-source platform for biological-image analysis. Nat Methods. 2012;9(7):676-82. doi: 10.1038/nmeth.2019. PubMed PMID: 22743772; PubMed Central PMCID: PMCPMC3855844.

19. Tashev SA, Parsons D, Hillman C, Harris S, Lofthouse EM, Goggin P, et al. Folding of the syncytiotrophoblast basal plasma membrane increases the surface area available for exchange in human placenta. Placenta. 2021;117:57-63. Epub 2021/11/13. doi: 10.1016/j.placenta.2021.11.002. PubMed PMID: 34768170.

20. Harris SE, Matthews KS, Palaiologou E, Tashev SA, Lofthouse EM, Pearson-Farr J, et al. Pericytes on placental capillaries in terminal villi preferentially cover endothelial junctions in regions furthest away from the trophoblast. Placenta. 2021;104:1-7. Epub 2020/11/16. doi: 10.1016/j.placenta.2020.10.032. PubMed PMID: 33190063; PubMed Central PMCID: PMCPMC7921774.

21. Mizushima N, Yoshimori T, Levine B. Methods in mammalian autophagy research. Cell. 2010;140(3):313-26. Epub 2010/02/11. doi: 10.1016/j.cell.2010.01.028. PubMed PMID: 20144757; PubMed Central PMCID: PMCPMC2852113.

22. Mayor S, Parton RG, Donaldson JG. Clathrin-independent pathways of endocytosis. Cold Spring Harb Perspect Biol. 2014;6(6). Epub 2014/06/04. doi: 10.1101/cshperspect.a016758. PubMed PMID: 24890511; PubMed Central PMCID: PMCPMC4031960.

23. Cooke LDF, Tumbarello DA, Harvey NC, Sethi JK, Lewis RM, Cleal JK. Endocytosis in the placenta: An undervalued mediator of placental transfer. Placenta. 2021;113:67-73. Epub 2021/05/18. doi: 10.1016/j.placenta.2021.04.014. PubMed PMID: 33994009.

24. Jones CJ, Fox H. Ultrastructure of the normal human placenta. Electron Microsc Rev. 1991;4(1):129-78. PubMed PMID: 1873486.

25. Rescigno M, Urbano M, Valzasina B, Francolini M, Rotta G, Bonasio R, et al. Dendritic cells express tight junction proteins and penetrate gut epithelial monolayers to sample bacteria. Nat Immunol. 2001;2(4):361-7. Epub 2001/03/29. doi: 10.1038/86373. PubMed PMID: 11276208.

26. Murrieta-Coxca JM, Aengenheister L, Schmidt A, Markert UR, Buerki-Thurnherr T, Morales-Prieto DM. Addressing microchimerism in pregnancy by ex vivo human placenta

perfusion. Placenta. 2021;117:78-86. Epub 2021/11/14. doi: 10.1016/j.placenta.2021.10.004. PubMed PMID: 34773744.

27. Palaiologou E, Goggin P, Chatelet DS, Lofthouse EM, Torrens C, Sengers BG, et al. Serial block-face scanning electron microscopy of erythrocytes protruding through the human placental syncytiotrophoblast. Journal of anatomy. 2017;231(4):634-7. Epub 2017/07/18. doi: 10.1111/joa.12658. PubMed PMID: 28714092; PubMed Central PMCID: PMCPMC5603844.

28. Day PE, Cleal JK, Lofthouse EM, Hanson MA, Lewis RM. What factors determine placental glucose transfer kinetics? Placenta. 2013;34(10):953-8. doi: 10.1016/j.placenta.2013.07.001. PubMed PMID: WOS:000330331500016.

29. Wagner R, Modla S, Hossler F, Czymmek K. Three-dimensional analysis and computer modeling of the capillary endothelial vesicular system with electron tomography. Microcirculation. 2012;19(6):477-84. Epub 2012/03/23. doi: 10.1111/j.1549-8719.2012.00181.x. PubMed PMID: 22435898.

30. Palaiologou E, Goggin P, Chatelet DS, Ribeiro de Souza R, Chiu W, Ashley B, et al. Serial block-face scanning electron microscopy reveals novel intercellular connections in human term placental microvasculature. Journal of anatomy. 2020;237(2):241-9. Epub 2020/04/04. doi: 10.1111/joa.13191. PubMed PMID: 32242928; PubMed Central PMCID: PMCPMC7369196.

31. King BF. Ultrastructural evidence for transtrophoblastic channels in the hemomonochorial placenta of the degu (Octodon degus). Placenta. 1992;13(1):35-41. Epub 1992/01/01. PubMed PMID: 1502135.

32. Ferreira APA, Boucrot E. Mechanisms of Carrier Formation during Clathrin-Independent Endocytosis. Trends Cell Biol. 2018;28(3):188-200. Epub 2017/12/16. doi: 10.1016/j.tcb.2017.11.004. PubMed PMID: 29241687.

33. Atkinson DE, Robinson NR, Sibley CP. Development of passive permeability characteristics of rat placenta during the last third of gestation. The American journal of physiology. 1991;261(6 Pt 2):R1461-4. Epub 1991/12/01. doi: 10.1152/ajpregu.1991.261.6.R1461. PubMed PMID: 1750569.

34. Collins MC, Ramirez WF. Transport through polymeric membranes. J Phys Chem 1979;83:2294–301. doi: https://doi.org/10.1021/j100480a022.

Figures and tables

Table 1: Estimated number of pores per gram required to explain the experimentally observed placental permeability surface area products.

	D ($m^2\ s^{-1}$)	PS_{pore} ($m^3\ s^{-1}$)	$PS_{placenta}$ ($m^3\ s^{-1}\ g^{-1}$)	number of pores (g^{-1})
Inulin*	2.6×10^{-10}	2.20×10^{-18}	0.28×10^{-10}	13×10^{6}
CrEDTA*	7.0×10^{-10}	5.92×10^{-18}	1.06×10^{-10}	18×10^{6}
Mannitol*	9.9×10^{-10}	8.37×10^{-18}	2.50×10^{-10}	30×10^{6}
Creatinine**	12.9×10^{-10}	10.9×10^{-18}	6.41×10^{-10}	59×10^{6}

*Placental permeability surface area product data taken from Bain *et al.* (1990) [6] and diffusion coefficients from Atkinson *et al.* (1991) [33]. ** Permeability surface area product calculated based on Cleal *et al.* (2007) and diffusion coefficient from Collins *et al.* (1979) [34].

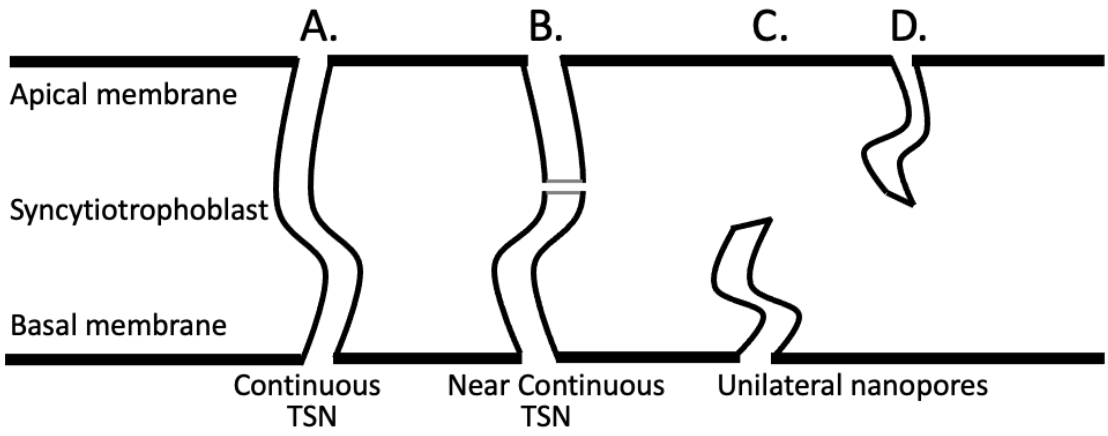

Figure 1, Classification of nanopores found in human placental syncytiotrophoblast. A, continuous TSNs connecting the apical and basal membrane without any breaks. **B,** near-continuous TSNs with sections connected to the apical and basal plasma membranes but contained discontinuities where no clear connection could be observed but the ends of the discontinuous sections were adjacent. **C & D.** Unilateral nanopores were ultrastructurally similar to TSNs but opened from either the apical or basal plasma membrane but without any apparent connection to the opposing membrane.

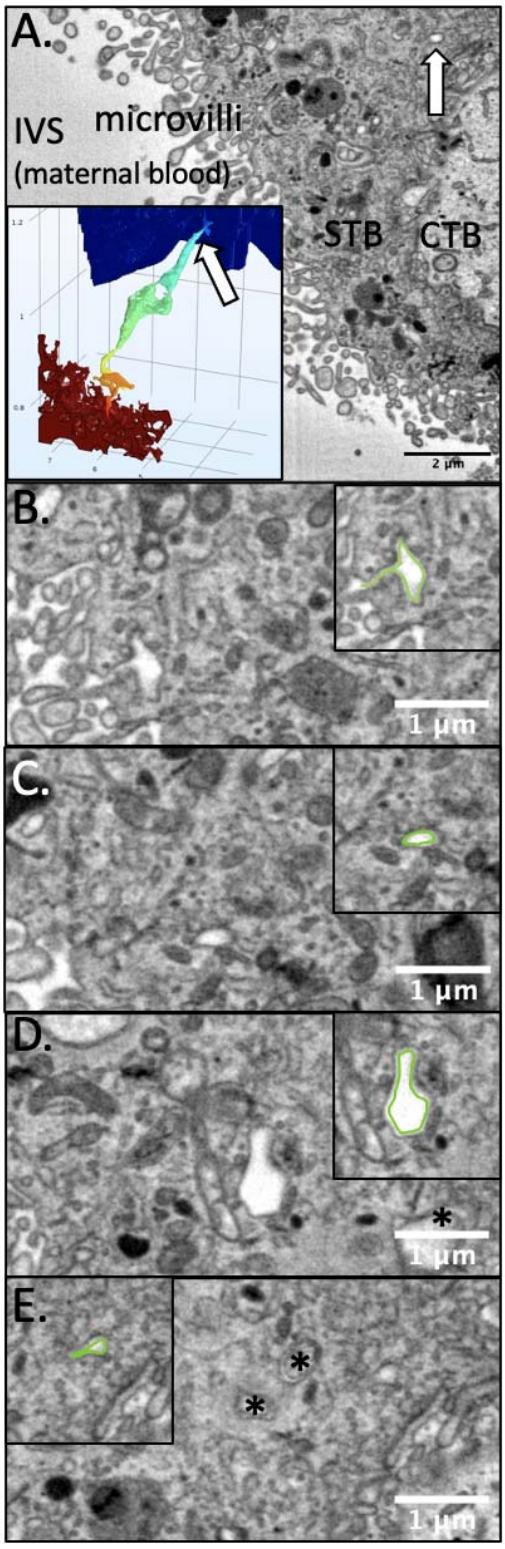

Figure 2, SBF SEM serial sectioning allows identification of TSNs crossing the human placental syncytiotrophoblast. A) An SBF SEM image showing a cross section of the syncytiotrophoblast (STB) from the maternal intervillous space (IVS) to the underlying cytotrophoblast (CTB). Within this image a cross section of a nanopore can be seen (white arrow) illustrating how difficult it would be to identify these structures from individual 2D images. The inset shows the nanopore reconstructed in 3D from 44 consecutive sections with the white arrow indicating where the section comes from and modelled solute concentration indicated by colour from high (red) to low (blue). **B)** the apical opening of the TSN with the inset showing this highlighted in green. **C)** A thin region of nanopore with the inset showing this highlighted in green. **D)** a dilated region of the nanopore with the inset showing this highlighted in green. In B, C and D the nanopore has a low electron density consistent with a fluid filled pore **E)** A region of nanopore where the lumen has a higher electron density than in other regions. The inset showing this cross section of the nanopore highlighted in green. This region is close to the end of the nanopore and the cytotrophoblast boundary can be seen bottom left. * Indicate inclusion bodies. A movie showing the nanopore highlighted in individual slices can be seen in the supplemental movie 1).

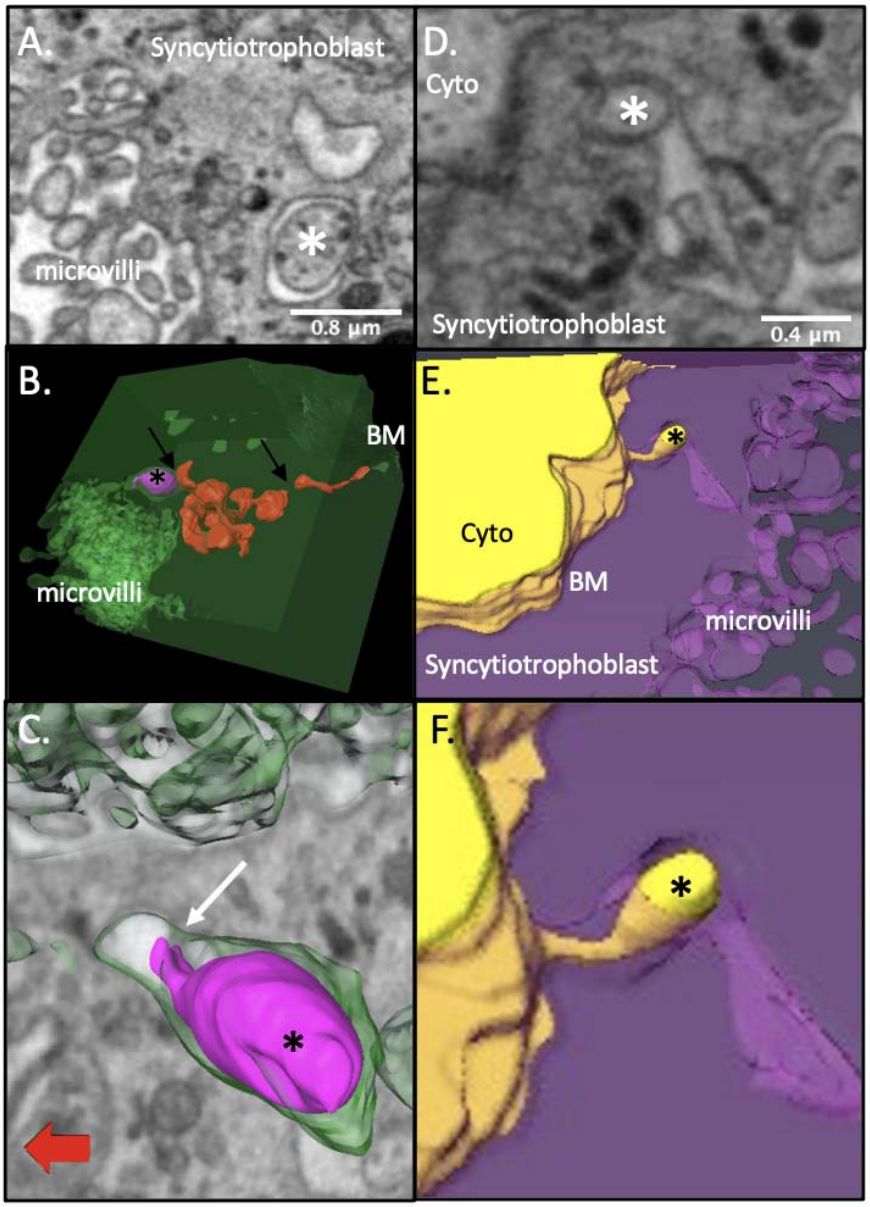

Figure 3, **Examples of TSN inclusions formed from engulfed syncytiotrophoblast or cytotrophoblast. A-C**) an apical nanopore inclusion body (*) was observed which appeared to be derived from the trophoblast (green). **A)** shows a SBF SEM image containing a cross section of a TSN inclusion. **B)** shows the same inclusion (pink) in 3D within a complex near-continuous TSN (red). This TSN has several discontinuities indicated by black arrows but gives the appearance of being part of a trans-syncytial network even if it does not form a complete pore. **C)** shows a higher power image of the inclusion which is continuous with the syncytiotrophoblast (green) via a small stalk (white arrow). **D-F)** An example of a TSN inclusion which is derived from the underlying cytotrophoblast (yellow). **D)** shows a SBFSEM image of the cytotrophoblast derived inclusion. **E)** shows the nanopore inclusion within a TSN with a relatively simple tubular structure. **F)** shows a higher power image of the cytotrophoblast derived inclusion.

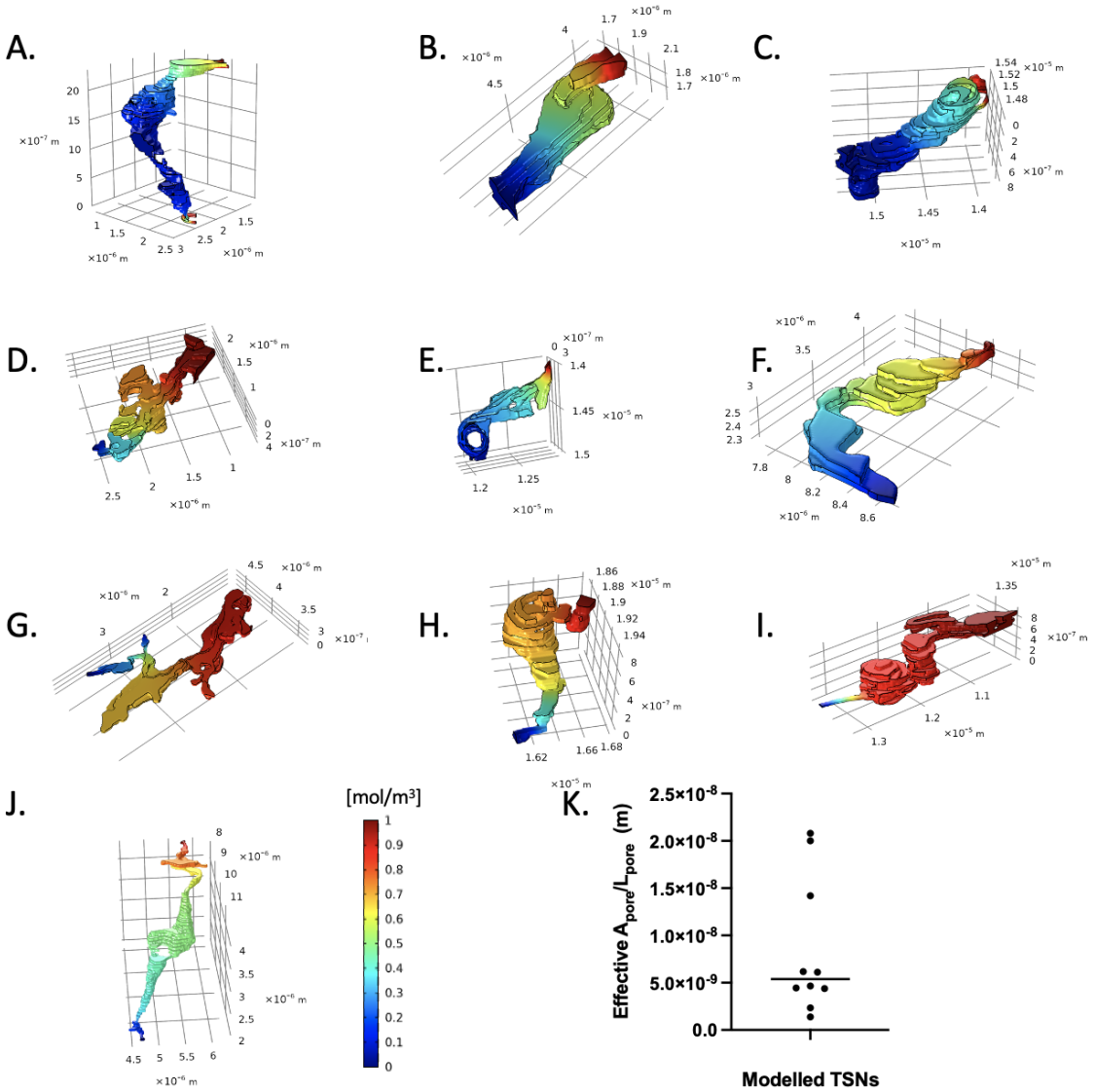

Figure 4, **Modelled solute concentration gradients within the continuous TSNs.** High concentrations (red) were applied to the maternal facing TSN opening, and concentration gradients are shown for diffusion through the channel. The molecular flux associated with these gradients was used to calculate the effective cross sectional surface area used to calculate permeability. **A-J)** show the nanopores presented in order of calculated permeability from highest to lowest. The apical opening is presented on top right and basal openings on the bottom or left. The TSN shown in A is a double pore with four apical and basal openings and a connection on the basal side which accounts for its higher permeability despite its longer length. Blind ends are present in D, I and G. TSN A has two openings to the microvillous membrane and two openings to the basal membrane of the syncytiotrophoblast. **J)** shows a scatterplot showing the distribution of permeabilities with the line indicating the median value.

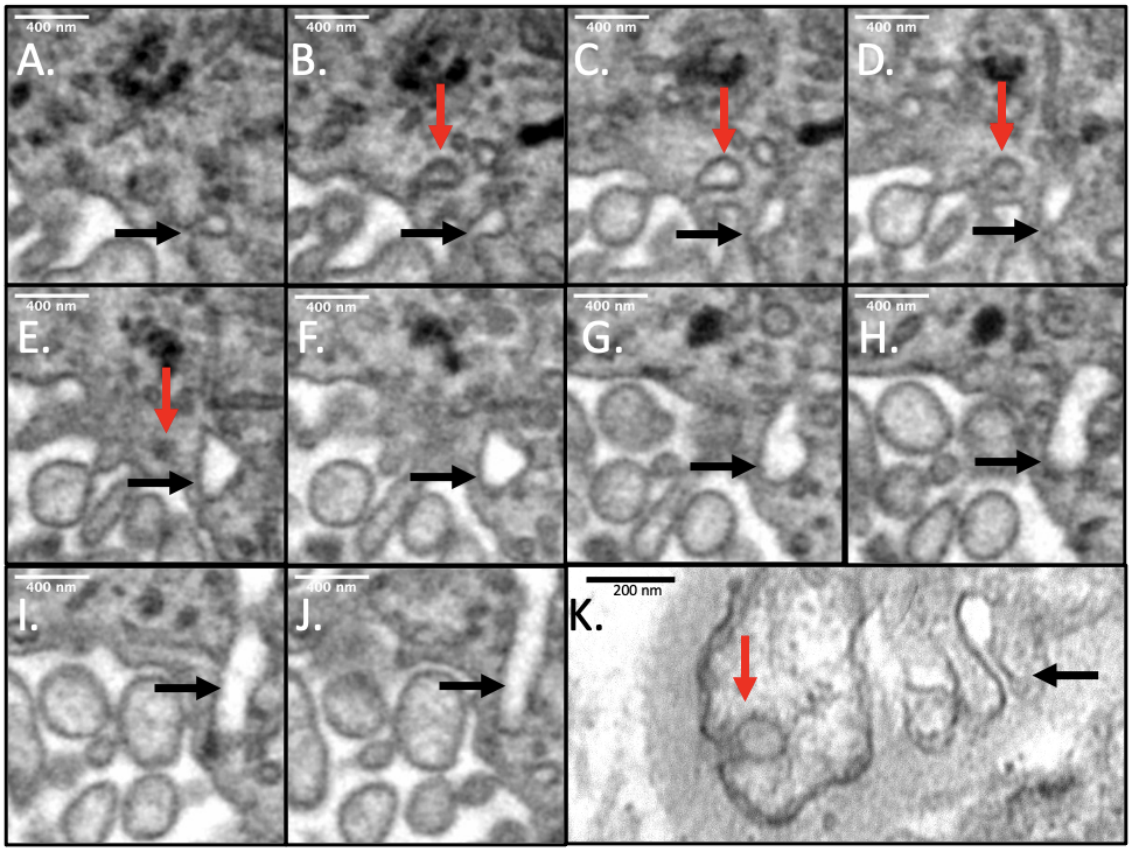

Figure 5, **Comparison of endocytic vesicle and TSN openings on the apical and basal membranes of the placental syncytiotrophoblast. A-J** serial SBFSEM images (50 nm apart) showing a flask shaped invagination forming the opening to a TSN (black arrow), alongside a vesicle (seen in B-E, red arrows) In these images the microvilli are bottom left. **K.** TEM image of syncytiotrophoblast basal membrane showing an endocytic vesicle with dynamin spirals (red arrow) near an opening characteristic of a TSN (black arrow).

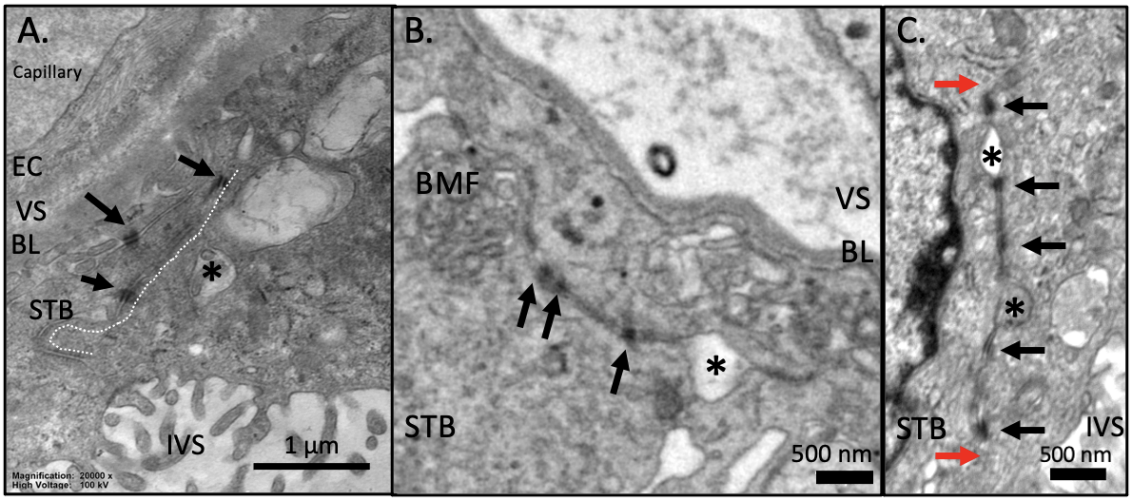

Figure 6, Desmosome associated nanopores. A) a TEM image of a desmosome associated nanopore traversing most of the width of the syncytiotrophoblast (white dotted line) and associated with dilation typical of TSNs (indicated by an *). **B)** an SBF SEM image of a desmosome associated nanopore connecting basal membrane folds to a TSN like opening (*). **C)** A TEM image of a desmosome associated nanopore which begins and ends in the same field of view (red arrows). This demonstrates that it is not a cell-cell junction as if this were the case it would need to intersect 2 sides of the image or be a circle. This channel contains an empty TSN like dilation (top*) and one which contains inclusion material (bottom*). EC = endothelial cell, VS = villous stroma, BL = basal lamina, STB = syncytiotrophoblast, BMF = basal membrane folds. IVS = intervillous space.